An Embedded System Remotely Driving Mechanical Devices by P300 Brain Activity

D. De Venuto, V. F. Annese, G. Mezzina
Dept. of Electrical and Information Engineering (DEI), Politecnico di Bari, Italy
Via Orabona 4, 70125 Bari – Italy

Abstract— **In this paper we present a P300-based Brain Computer Interface (BCI) for the remote control of a mechatronic actuator, such as wheelchair, or even a car, driven by EEG signals to be used by tetraplegic and paralytic users or just for safe drive in case of car. The P300 signal, an Evoked Related Potential (ERP) devoted to the cognitive brain activity, is induced for purpose by visual stimulation. The EEG data are collected by 6 smart wireless electrodes from the parietal-cortex area and online classified by a linear threshold classifier, basing on a suitable stage of Machine Learning (ML). The ML is implemented on a µPC dedicated to the system and where the data acquisition and processing is performed. The main improvement in remote driving car by EEG, regards the approach used for the intentions recognition. In this work, the classification is based on the P300 and not just on the average of more not well identify potentials. This approach reduces the number of electrodes on the EEG helmet. The ML stage is based on a custom algorithm (t-RIDE) which tunes the following classification stage on the user's "*cognitive chronometry*". The ML algorithm starts with a fast calibration phase (just ~190s for the first learning). Furthermore, the BCI presents a functional approach for time-domain features extraction, which reduces the amount of data to be analyzed, and then the system response times. In this paper, a proof of concept of the proposed BCI is shown using a prototype car, tested on 5 subjects (aged 26 ± 3). The experimental results show that the novel ML approach allows a complete P300 spatio-temporal characterization in 1.95s using 38 target brain visual stimuli (for each direction of the car path). In free-drive mode, the BCI classification reaches 80.5 ± 4.1% on single-trial detection accuracy while the worst-case computational time is 19.65ms ± 10.1. The BCI system here described can be also used on different mechatronic actuators, such as robots.**

Keywords — BCI; P300; Machine Learning; Classification;

I. INTRODUCTION

A Brain-Computer Interface (BCI) is a system providing a direct communication channel between human brain and an external device, generally via computer. Since the BCI systems can potentially improve the quality of life of paralytic, tetraplegic and motor impaired people, the scientific research in this field is experiencing an exponential growth. BCIs can be categorized basing on the particular brain activity pattern to be detected, which are sensorimotor rhythms (SMR), amplitude modulation of slow cortical potentials (SCP), visual cortex potentials (VEPs) or Event-Related Potentials (ERPs) [1]. The ERP-based BCI systems are mainly based on the P300, i.e. a large positive deflection in EEGs reaching its peak around 300ms after the excitation event. It reflects the stage of stimulus classification and it is excitable by the oddball paradigm, in which low-probability target items are mixed with high-probability not-target (or "standard") items [2, 3]. Differently from SMR and SCP based BCI, the ones based on P300 do not require intensive machine learning (ML), because the P300 component results from endogenous attention-based brain function. Although individual differences in P300 latency and amplitude have also been reported in [4], this happens for every human being, with a high degree of repeatability. In the field of BCI for locomotion, Grychtol et al. [5] demonstrated the possibility to control a wheelchair by brainwaves with a success rate of 72% ± 27% (depending on the subject). Ortner et al [6], instead, developed a mind-controlled prosthetic hand through a VEP-based BCI reaching a success rate of 78% ±10%. Differently, the research activity in BCI applied to vehicles is still far from being mature. Luzheng Bi et al. [7] developed a display-based P300 BCI for destination selection in vehicles. However, despite the good accuracy (93.6% ± 1.6%), the system in [7] did not allow real-time navigation since the selection time was about 12s [7]. Furthermore, D. Gohring et al [8] reported the development of a semi-autonomous car controlled by BCI. Although the prototype in [8] allows the free-drive mode, the proposed BCI is based on SMR, requiring a very intensive training stage. Further P300-based BCIs have been implemented covering a wide range of applications: locomotion (i.e. wheelchairs [5], robot or neuro-prosthesis [6]), rehabilitation (i.e. the "Bionic Eye" [9]), communication (i.e. the P300 speller [10]), environmental control (i.e. the "Brain Gate" [11]) and entertaining (i.e. neuro-games [12]). In this context, this paper presents a P300-based BCI for the remote control of a mechatronic actuator overcoming the above-mentioned limits. A proof of concept of the proposed BCI is shown using a prototype car: we demonstrate that a user controls the vehicle in free-drive mode just by using brain signals, without need for any physical interaction. The main improvements of the proposed BCI with respect to the state of the art are: i) the development of the first P300-based mind-controlled vehicle to be used in free-drive mode; ii) a custom algorithm, t-RIDE [4], for the ML, which allows a complete P300 spatio-temporal characterization in only 1.95s using 38 target brain visual stimuli (for each addressable command); iii) functional approach for the classification based on spatio-temporal features extraction (FE). The FE stage allows fast interpretation of the user's intention (worst case: 19.65ms ± 10.1ms), keeping high success rate 80.5 % ±4.1 (tested on 5 subjects). The structure of the paper is described in the following. Section II outlines the architecture of the BCI, focusing on the neurophysiological implemented protocol and the pattern recognition strategy (ML and classification algorithms). Section III describes the development of the Prototype Car System (PCS) and its interfacing with the BCI. Section IV reports experimental results of the system carried out on 5 subjects. Section V concludes the paper with final observations.

978-3-9815370-8-6/17/$31.00 ©2017 IEEE

II. The Architecture

The architecture outlines a functional approach for a fast *synchronous* BCI, through a useful application such as mind-drive experience. The overall architecture (Figure 1) can be divided into two subsystems: the Brain Computer System (BCS) and the Prototype Car System (PCS). They are connected together through a Client-Server TCP/IP communication protocol. The BCS is made up by the hardware acquisition system (wireless EEG headset station) and by the algorithm that interprets the user/driver intentions and communicates them to the PCS. The PCS is made up by an acrylic prototype car, equipped by a camera, two DC motors, three servomotors (two for camera and one for steering), managed by a programmed µPC (Raspberry Pi 2). The PCS sends a real-time video to the BCS while receiving commands for the control of DC motors and servomotors.

A neurophysiological protocol allows the interaction between human brain and BCS by using an "ad-hoc" locally generated visual stimulation that evocates the P300 potential. To tune the system on the particular user, a Machine Learning stage (ML) is needed. During the ML, the BCS proposes the user a visual task which lasts only 190s (for each direction), achieving the system calibration. A custom algorithm, the tuned-Residue Iteration Decomposition (t-RIDE) [4], which characterizes the P300 waveform and extracts all the parameters to be used for the real time classification stage, performs the ML. When the classifier recognizes and validates the user intention, the BCS provides a flag signal to the PCS. Afterwards, PCS runs a pre-compiled set of scripts that drive the steering, the camera servomotors and the DC motors.

A. Neurophysiological Protocol and Instrumentations

Stimulation Protocol. The stimulation protocol is designed according to the odd-ball paradigm: the user is asked to identify and mentally count the occurrence of a visual rare stimulus, filtering out irrelevant stimuli. There are four delivered visual stimuli, individually and randomly flashing on a display (25% occurrence probability) with an inter-stimuli time of 1s. Each stimulus persists on the screen for 200ms. Each stimulus is related to a command to be sent to the PCS. When the user focuses his attention on a particular stimulus (so he is expressing a direction), the stimulation can be considered a classical binary discrimination problem: the P300 can be detected related to the selected stimulus, allowing the user's intention interpretation. Figure 2 shows a sequence of driving environment snapshots provided by the BCS to the user. For instance, if the user wants to turn left, from his position, the target items in Fig. 2.a are the stimuli to be counted, while the other blinking stimuli are the not-target. Neurophysiological studies [13] reveal that P300 latency and amplitude are related to the saliency of stimulus (in term of color, contrast, brightness, duration, etc.). For this aim, the BCS associates to each direction different shapes and colors, in sharp contrast to each other (see Figure 2).

Hardware. A 32-channels wireless headset acquires EEG signals with active electrodes (conditioning integrated circuit are embedded in the electrode performing amplification,

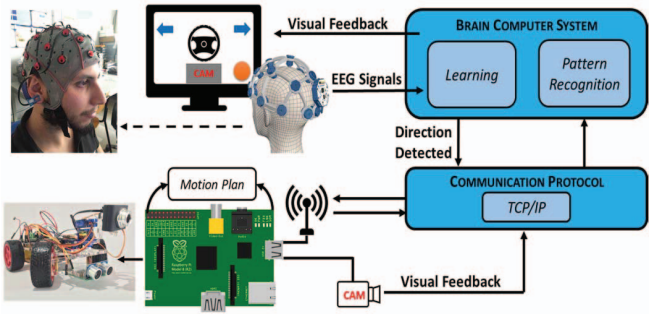

Fig. 1. Schematic overviewe of the developed BCI architecture .

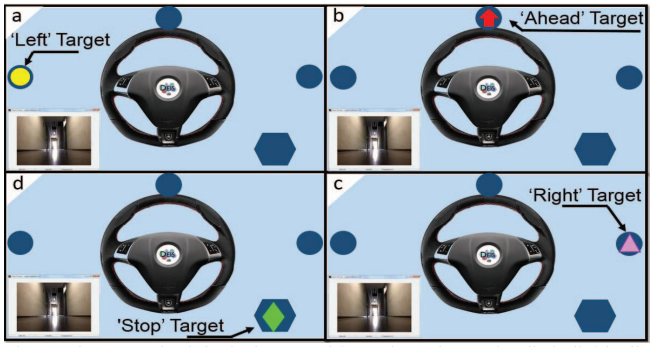

Fig. 2. The neurophysiological protocol is made up by 4 stimuli individually and randomly flashing on a display. Each stimulus is related to a particular command i.e. turn left (a), turn right (c), go ahead (b) and stop (d).

Filtering and digitalization) as the one used in [14, 20]. The locations of the electrodes have been chosen according to previous P300 studies [13] and, in a later stage, reduced in number basing on the relevance in experimental conditions (as highlighted in Figure 3.a). According to the international 10-20 standard, the EEG recordings have been performed using six electrodes (C_Z, C_{P1}, C_{P2}, P_3, P_Z, P_4 – in red in Fig. 3.a) referenced to AF_Z electrode (in orange in Fig.3.a) and right ear lobe (A_2 – in green in Fig. 3.a) is used as ground. EEG signals are recorded with sampling frequency of 500Hz, 24-bit resolution, ±187.5mV input range and filtered using a bandpass (Butterworth, 8^{th} order 2-30Hz) and power line notch filtered (Butterworth, 4^{th} order 48-52Hz - embedded into the front-end) [21-26] . The recording scheme is monopolar. The EEG signals are recorded during the drive and are synchronized with the delivered stimuli by the gateway. In the experimental evaluation, the gateway has been assumed as a PC (Intel i5, RAM 8 GB, 64 bit) which collects EEG data, generates and delivers the stimulation.

Pre-processing. Aiming to reduce both noise and artifacts (eyes and head movements), data pre-processing is performed on each channel but, for clarity, the pre-processing chain is outlined only for a single one. The acquired signal is low-pass filtered (Butterworth, 6^{th} order, f_{3dB} = 15Hz) and aligned to the stimulus signal. Subsequently, the EEG signal is decomposed in trial of 1s. Each trial starts as soon as the rising edge of the stimulation arrives. Finally, trials are fitted in a 6^{th} order polynomial (with bi-square Weights). The resulting curve is subtracted from the EEG signal that is then centered (offset cancellation) and normalized.

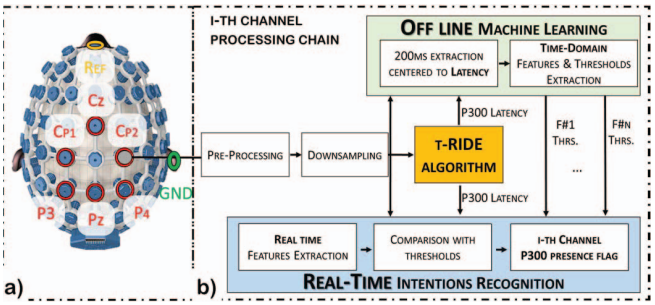

Fig. 3. a) Channels of interest (in red) according to the international system 10-20. In yellow the nasion reference and in green the ear-lobe ground. b) Illustration of the processing chain for a single channel.

TABLE I. FEATURES COMPUTATION FORMALIZATION

Feature	Feature Computation
Convexity (f1)	$f_1 = \begin{cases} 1 & \leftrightarrow \quad \sum_{i=1}^{\left(\frac{ns}{2}\right)-1} \frac{\partial x(i)}{\partial i} \geq \sum_{i=\left(\frac{ns}{2}\right)+1}^{ns} \frac{\partial x(i)}{\partial i} \\ 0 & otherwise \end{cases}$
Triangle area (f2) [μV·ms]	$f_2 = 0.5 \cdot \begin{vmatrix} x_1 & y_1 & 1 \\ x_2 & y_2 & 1 \\ x_3 & y_3 & 1 \end{vmatrix}$
Symmetry (f3)	$f_3 = 1 - \left\lvert \frac{2}{ns-1} \sum_{i=1}^{ns} [x(i) - x(ns-i)] \right\rvert$
Peak to Max distance (f4) [μV]	$f_4 = \frac{\frac{(ns+1)}{2} - \left\lvert \frac{(ns+1)}{2} - index(\max(x)) \right\rvert}{\frac{(ns+1)}{2}}$
Direction changes (f5)	Custom code which count the zero crossing of the derivative signal

[1] x(i) = sampled ERP waveform; [2] ns = number of data samples; [3] (x_1, y_1) and (x_2, y_2) are the minimum values of the P300 brainwave, on the left and on the right side of the learned latency. (x_3, y_3) are the coordinates of maximum value of the extracted samples.

B. Pattern Recognition Strategy

Figure 3.b outlines the processing chain for a single channel from the acquisition to the generation of the P300 presence/absence signal. The first step of this strategy is to train the system via offline experiment with a learning stage (green branch in Fig. 3.b). Once this stage is over, the real-time classifier (blue branch in Fig. 3.b) can operate.

Machine Learning Stage. The ML step bases its operation on a tuned version of Residue Iteration Decomposition (t-RIDE) approach, developed in previous works and widely treated in [4]. t-RIDE allows P300 extraction basing on a liner superposition model of the single-trials EEG by decomposing the P300 into stimulus-locked and cognitive-locked components [4]. t-RIDE allows fast P300 characterization for each channel in terms of waveform, amplitude, latency and topographic distribution. The t-RIDE extracted P300 pulse undergoes a phase of Features Extraction (FE) to be used as 'golden reference' by the classifier. According to specialized medical staff P300 visual inspection guidelines, five features have been selected. They consider the most peculiar P300 shape information in time-domain, in order to exalt the differences between target and not-target response. Five features have been selected: i) Convexity (i.e. the convexity of the P300 wave centered on the expected latency value); ii) Triangle Area (i.e. the integral of the curve approximated to a triangle); iii) Simmetry (i.e. the symmetry degree of the signal with respect to the expected latency); iv) Peak-to-Peak distance (i.e. Euclidean distance measure between the voltage peak of the single trial with respect to the expected one); v) Number of slope changes (i.e. the number of slope sign changes for the considered waveform derivative). Table I summarize the procedure for the features calculation. The FE for the ML is performed offline, on the same acquired raw data and performed on single-trials (for both targets and not-targets). The features distributions are analyzed by a statistical method that extracts, for each feature, the 25th and 75th percentiles and median value. The percentiles values allow to obtain the thresholds definition, while the median value delivers a set of weights (one set for each channel) to be used by the classifier. These weights are assigned evaluating the subtraction between the median value of the j-th feature vector referred to the target responses and the not-target ones. The learning step assigns their values in descending order starting from 0.3 for the best feature to 0.1 for the worst one. The remaining 3 features assume decreasing weights with 0.05 steps between 0.3 and 0.1. These values allow obtaining a sum that provides a maximum of 1. At the end of the ML and FE phase, the following subject-depending parameters have been learned by the BCS:

1. **UP** $\in R^{5x6}$: $up_{i,j}$ = upper threshold for i-th feature (the 75th percentile) referred to the j-channel.
2. **DN** $\in R^{5x6}$: $dn_{i,j}$ = lower threshold for i-th feature (the 25th percentile) referred to the j-channel.
3. **W** $\in R^{5x6}$: $w_{i,j}$: i-th weight referred to the j-channel.
4. **S** $\in R^{6}$: s_j = responsivity (detection rate) of the j-th channels.
5. **L** $\in R^{6}$: l_j = expected P300 latencies for the j-th channel.
6. **A** $\in R^{6}$: a_j = expected P300 amplitude for the j-th channel.

Real-time Classification. The classification is conducted on a down-sampled (from 500sps to 100sps) and windowed (M samples centered on the expected latency, M = 20 ~200ms) version of EEG trial, with the aim of reduce the computational times. The A matrix delivers a first step of acquired data validation. Indeed, in order to avoid that artifacts affect the results, data are validated only if they do not exceed the limits imposed by the matrix. As soon as a new stimulus occurs, the BCS performs the FE on the single-trial for each channel basing on **L**. This leads to the extraction of an online features matrix **f** $\in R^{5x6}$ where its generic element $f_{i,j}$ expresses the value of the i-th feature on the j-th channel. The classifier adopts the following decisional rule:

$$F_{i,j} = \begin{cases} 0 & \leftrightarrow \quad f_{i,j} < dn_{i,j} \\ 0.5 & \leftrightarrow \quad dn_{i,j} \leq f_{i,j} \leq up_{i,j} \\ 1 & \leftrightarrow \quad f_{i,j} > up_{i,j} \end{cases} \tag{1}$$

This procedure leads to the creation of the matrix **F** $\in R^{5x6}$. A weighted sum of F defines the presence of the P300 on the j-th channel, through the calculation of the vector R$\in R^6$, where the generic element is:

$$r_j = w_{1,j} \cdot F_{1,j} + \ldots + w_{5,j} \cdot F_{5,j} \text{ for } j = 1, 2, \ldots, 6 \tag{2}$$

Afterwards, the classifier adopts a second decision rule to decide the presence/absence of P300 on the j-th channel:

$$y_j = \begin{cases} 0 & \leftrightarrow \quad r_j \leq y_t \\ 1 & \leftrightarrow \quad r_j > y_t \end{cases} \tag{3}$$

Where y_j is the generic element of **Y** $\in R^6$ and y_t is a decision threshold set to 0.5. In order to overcome the threshold (y_t value), at least 3 features need to be detected on the j-th channel. The classification ends with the topographical validation: if there is a simultaneous P300 wave detection on 5 out of 6 monitored channels, the classifier validates the P300 presence (with particular attention to the channels which deliver high

detection rate and reported in the vector **S**). At the end of the classification step, the BCS wirelessly communicates to the PCS a 2 bits code informing Raspberry about the actuation.

III. The Prototype Car

The schematic of the developed prototype car is presented in figure 4. A nominal supply voltage of 7.4 V is realized by using two 3.7V batteries (Panasonic 18650). Using a DC-DC converter (XL-1509), this voltage is stabilized to 5V, delivering the power supply for the entire prototype car. A Wi-Fi antenna, an USB camera and a SD card equip the Raspberry Pi 2 (Model B+), which represent the control unit of the PCS. The obstacle detection and its avoidance, as well as the management of the servomotors and DC motor power control are the three fundamental aspects of the navigation. They are fully entrusted to the Raspberry set of scripts.

The obstacle detection and avoidance is based on three ultrasonic proximity sensors (HC-SR04): one is positioned frontally while the others sideways. The 'Trig' pins of the ultrasonic sensors are driven by a single output Raspberry pin and triggered at 10Hz with a pulse wave of 10µs. The sensors response delivered on their 'Echo' pin are connected to three different Raspberry input pins. The presence/absence of obstacles are continuously monitored by running a local generated Python script. When an obstacle is detected ahead with a distance lower than 50cm, the prototype car brakes. While if a side obstacle is detected, Raspberry alerts the BCS that adapts the provided visual protocol, which it will not allow the user to curve on that direction.

The DC motor power control is managed by Raspberry Pi using an h-bridge (L298N): GPIO pins controls the enable pins of the L298N ('ena', enb') using pulse with modulation (PWM).

The servomotor management is entrusted to the PWM module (PCA 9685). There are three servomotor: while the first one manages the prototype car direction (and is controlled by the BCS), the other ones control the orientation of the USB camera, which streams a real-time video to the BCS.

IV. Results

The architecture has been tested on a dataset from 5 subjects (aged 26±3) with a high degree of homogeneity in terms of education, age and lifestyle. The subjects performed at first the learning protocol and, subsequently, the real-time prototype car control. In the real-time validation, we refer to classification accuracy, calculated using the following equation:

$$ca = \frac{TG+nTG}{TT} \cdot 100 \quad (4)$$

where TG and nTG are the number of – respectively - target and not-target stimuli pointed by the user and correctly detected; TT is the total number of delivered stimuli.

A. Offline Learning

The leaning stage is performed offline: firstly, the user performs a neurophysiological test in which he is asked to count in mind 38 target stimuli (i.e. ~190s) for each direction (fig. 2). EEG data are acquired and processed by t-RIDE for P300 extraction. Figure 5 presents a typical down-sampled version of the responses to target stimuli (i.e. the P300 in blue) against not-target ones (in red) for all the channels.

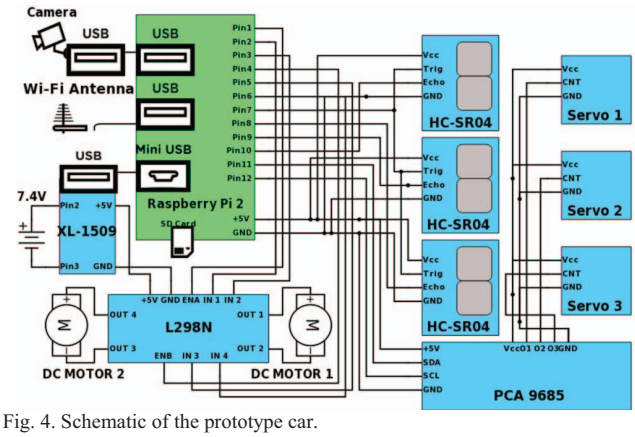

Fig. 4. Schematic of the prototype car.

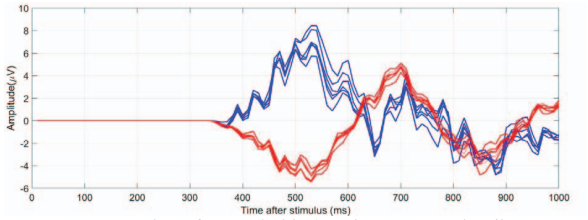

Fig. 5. t-RIDE extraction of P300 (in blue) and not-target stimuli response on all the channels.

The P300 waveforms extraction is performed by t-RIDE. The subsequent phase of FE performed on the extracted P300 waveform defines a set of upper thresholds (**UP**), lower thresholds (**DN**), amplitude reference values (**A**), latency reference values (**L**), weight sets (**W**), and spatial responsivity (**S**) for each monitored channel. In table II, the complete characterization of the dataset is presented. For clarity, the numerical values are presented in the form of mean ± std. deviation on all the 6 channels. Figure 6 proposes two demonstrative diagrams of the learning stage (in blue the upper thresholds and in red the lower ones). The subfigure 6.a presents the channel-to-channel variability of a single feature (i.e. f_2 = triangle area): the deep variability of the same feature computed on different channels shows that the use of different thresholds for the different channels is valid and it is not redundant. Fig. 6.b presents an example of thresholds learning for a single channel. The complete learned feature set is thus passed to the classifier, which uses them to online apply its decisional criteria.

B. Online Classification Validation

The online validation approach included two different tests: i) single direction repetitive selections and ii) pattern recognition. In the first approach, the user is asked to select repeatedly the target in fig. 2.d ('stop target'). The reached classification accuracies computed in these conditions are (see figure 7): sub1: 73.68 ± 5.3 %; sub2: 83.71 ± 4.6 %; sub3: 80 ± 3.1 %; sub4: 81.30 ± 4.8%; sub5: 83.84 ± 5.8%. The best classification accuracy achieved is 89.64%, while the worst one is 73.68%. The analysis demonstrated a channel-to-channel accuracy modulation: the channels with highest accuracy are C_z and P_z (i.e. Ch1 and Ch5, respectively), performing – respectively – 86.2% and 88.3% (average on all the subjects).

TABLE II. COMPLETE RESULTS FROM THE LEARNING ON THE ENTIRE DATASET

		Sub 1	Sub 2	Sub 3	Sub 4	Sub 5
A (μV)		10.6±0.7	9.6±0.4	11.2±0.57	10.0±0.93	9.5±1.06
L (ms)		510±107	434±10	569±47	383±7	414±45
f1*	UP	0.5±0	0.5±0	0.5±0	0.5±0	0.5±0
	DN	0.5±0	0.5±0	0.5±0	0.5±0	0.5±0
f2 (μV·ms)	UP	125.5±24.8	84.9±18.1	65.6±12.9	44.5±11.9	38.7±8.8
	DN	39.6±12.3	44.8±2.2	19.7±1.9	18.8±1.9	26.6±6.86
f3*	UP	0.68±0.01	0.68±0.03	0.68±0.03	0.67±0.03	0.65±0.02
	DN	0.43±0.09	0.23±0.07	0.19±0.10	0.43±0.14	0.36±0.08
f4 (ms)	UP	0.31±0.08	0.31±0.14	0.35±0.23	0.33±0.07	0.33±0.12
	DN	0.11±0.04	0.07±0.05	0.15±0.07	0.25±0.03	0.24±0.03
f5	UP	7.8±0.41	7.7±0.82	8±0.63	7.17±0.41	6.17±0.75
	DN	1.67±0.81	2.2±0.41	2.33±0.81	4.00±1.26	4.50±1.38

* Adimensional features. All the values are expressed as mean ± standard deviation (calcuated on all the chns)

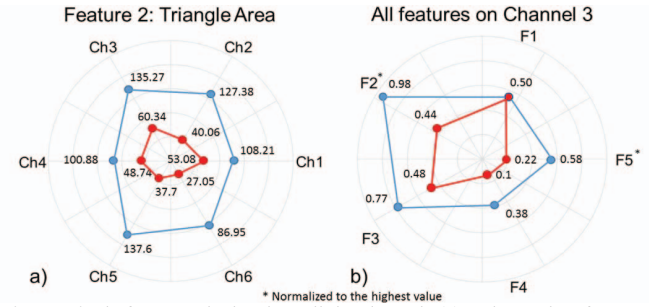

Fig. 6. Single feature calculated on all the channels (a) and complete features set calculated on single channel (b).

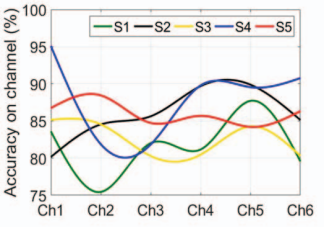

Accuracy for ↓ (%)				
Sub1	Sub2	Sub3	Sub4	Sub5
73.7 ± 5.3	83.7 ± 4.6	80 ±3.1	81.30 ± 4.8	83.84 ± 5.8

Mean accuracy on channels (%)					
Ch1	Ch2	Ch3	Ch4	Ch5	Ch6
86.2	81.3	82.6	84.9	88.3	83.7

Fig. 7. Subject-by-subject accuracy calculated on a single selection ('stop').

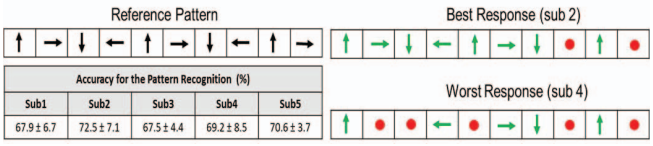

Fig. 8. Subject-by-subject accuracy and best/worst response to the pattern recognition test.

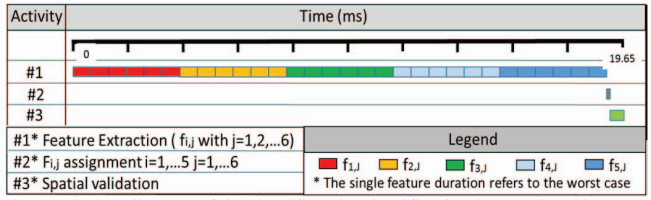

Fig. 9. Timing diagram of the classifier: the classification is completed in 19.65 ms (worst-case).

TABLE III. COMPARISON WITH THE CURRENT STATE OF THE ART

Work	BAP	Accuracy [%]	Selection Time [1]	No. of electrodes	ML Approach	Application
This work	P300	80.5 ± 4.1	1.03s	6	t-RIDE + FE	Vehicle
[7]	P300	93.6 ± 1.6	12s	8	PCA	Cursor
[6]	SVEP	78 ± 10	> 5.56 s	1	n.d.	Prosthesis
[5]	SMR	72 ± 27	n.d.	23	MI [3]	Wheelchair
[11]	SMR	< 95	2.5±0.17	96 [2]	MI [3]	Prosthesis

[1] Selection time = stimulus delivery time + classification time; [2] Signal acquired by ECoG using an array of 96 μelectrodes; [3] Motor Imagery; [4] n.d. = not defined.

The pattern recognition test consist in the selection of a known stream of direction. The reference pattern to be perform by the user is made up 10 commands covering all the addressable directions (outlined in figure 8). The users performed this test more than once. The performed accuracies in this test are (see figure 8): sub1: 67.9 ± 6.7 %; sub2: 72.5 ± 7.1 %; sub3: 67.5 ± 4.4 %; sub4: 69.2 ± 8.5 %; sub5: 70.6 ± 3.7%. The best pattern recognition is 8/10 while the worst response is 5/10 (50%).

C. *Timing*

The real-time operation requires the need for strict computational times. The present work overcomes the current state of the art in terms of computational times needed for both ML and classification. As demonstrated in [4], the novel algorithm t-RIDE is 1.6 times faster than ICA (P300 extraction on the same dataset is performed by t-RIDE in 1.95s and by ICA in 3.1s) reaching the convergence in 79 iterations.
Considering the hyper-dimensional classifier, the computational speed is guaranteed by the functional approach involving features extraction. The fixed communication latency from EEG headset and gateway is 14ms. The classifier needs to buffer 1s data after the stimulus in order to perform the computation. The worst-case computational time, for each feature extraction on single channel and single trial, was 0.653±0.32ms. The worst-case total time for the FE stage on 6 channels was 19.58±9.7ms. The successive definition of the matrix **F** was performed in 0.026±0.011ms on all the channels. The computational time (for 6 channels) for the spatial validation was 0.041±0.008ms. Given this computational details, the worst-case total time needed by the classifier to complete the classification for all the channels was 19.65± 10.1ms. Figure 9 details the time slots dedicated to the computation. It outlines that the FE stage is the most time consuming part of the process. The communication time between BCS and PCS is about 3.35ns (only 2 bits to be sent by Wi-Fi). As soon as Raspberry Pi receives the command, the actuation is performed in 3ms (worst-case). The overall architecture complete a single actuation (from EEG raw data acquisition triggered by stimulus delivery to PCS actuation) in 1.03s (worst-case).

D. *Discussion*

Table III proposes a comparison between this work and different BCIs reported in literature [5, 6, 7, 11, 27-29]. Although the accuracy of the proposed classification is lower than other approaches reported in literature (i.e. [7, 11]), its computational efficiency makes it of a particular utility for time-constrained application as the one we devised in this paper. In [11], a very high accuracy is reached (< 95 %) but it is due to an invasive technique, i.e. electrocorticography (ECoG), allowing higher spatial resolution during signal acquisition. In [7], higher accuracy is reached (93.6 ± 1.6 %) but the selection time is too high for real-time application (12s). Indeed, if compared to the actual state of the art, the present BCI exhibits a lower selection time (1.03s) reducing the number of monitored electrodes.

V. Conclusion

In this paper, we presented a novel P300-based Brain Computer Interface (BCI) for the online remote control of a mechanic actuator, such as a vehicle. The interpretation of the user's intention is based on the presence/lacking of P300 concurrently to a neurophysiological protocol: thanks to selective attention, the P300 is evoked only by the particular stimulus freely selected by the user. The architecture of the mind-controlled car is made up by a Brain Computer System (BCS), which interprets the user intention by fast classification algorithm, and by the Prototype Car System (PCS), controlled by Raspberry Pi 2 model B+, which performs the mechanic actuation. The main contribution of this paper concern the algorithmic processing for both Machine Learning (ML) and the fast online classification. The ML stage is performed by the custom algorithm t-RIDE and by feature extraction (FE). The system has been validated on a dataset of 5 subjects mind-controlling the prototype car. The average classification accuracy on a single direction was 80.51 ± 4.1 %. The average classification accuracy in the detection of a 10-direction pattern was 69.6 ± 1.9 %. The classifier completes its process on all the channels in 19.65± 10.1ms (worst-case).

References

[1] Fernando, L., Alonso, N., & Gomez-Gil, J. (2012). Brain computer interfaces, a review. Sensors, 12(2), pp.1211-1264.

[2] V.F. Annese, G. Mezzina, D. De Venuto. Towards Mobile Health Care: Neurocognitive Impairment Monitoring by BCI-based Game. IEEE SENSORS 2016. ISBN: 978-1-4799-8287-5. In Print. 2016.

[3] De Tommaso, M., Vecchio, E., Ricci, K., Montemurno, A., De Venuto, D., Annese, V.F. "Combined EEG/EMG evaluation during a novel dual task paradigm for gait analysis". Proceedings - 2015 6th IEEE International Workshop on Advances in Sensors and Interfaces, IWASI 2015, pp. 181-186. DOI: 10.1109/IWASI.2015.7184949. 2015.

[4] De Venuto, D., Annese, V.F., Mezzina, G. "Remote Neuro-Cognitive Impairment Sensing based on P300 Spatio-Temporal Monitoring". IEEE Sensors Journal, PP (99), art. no. 7562544. DOI: 10.1109/JSEN.2016.2606553. 2016.

[5] Grychtol, B., Lakany, H., Valsan, G., & Conway, B. A. (2010). Human behavior integration improves classification rates in real-time BCI. Neural Systems and Rehabilitation Engineering, 8(4), 362-368. doi: 10.1109/TNSRE.2010.2053218

[6] Ortner, Rupert, et al. "An SSVEP BCI to control a hand orthosis for persons with tetraplegia." IEEE Transactions on Neural Systems and Rehabilitation Engineering 19.1 (2011): 1-5.

[7] Bi, Luzheng, et al. "A head-up display-based P300 brain–computer interface for destination selection." IEEE Transactions on Intelligent Transportation Systems 14.4 (2013): 1996-2001.

[8] Göhring, Daniel, et al. "Semi-autonomous car control using brain computer interfaces." Intelligent Autonomous Systems 12. Springer Berlin Heidelberg, 2013. 393-408.

[9] Barnes, N. (2012). Visual processing for the bionic eye: Research and development of visual processing for low vision devices and the bionic eye.

[10] Farwell, L.A., & Donchin, E. (1988). Talking off the top of your head: Toward a mental prosthesis utilizing event-related brain potentials. Electroenceph Clin Neurophysiol, 70(6), 510-523. dio:1988;70:510–523

[11] Hochberg, L. R., Serruya, M. D., Friehs, G. M., Mukand, J. A., Saleh, M., Caplan, A. H., Branner, A., Chen, D., Penn, R. D., & Donoghue, J. P. (2006). Neuronal ensemble control of prosthetic devices by a human with tetraplegia. Nature Journal 442, 164–171.

[12] Nijholt, Anton. "BCI for games: A 'state of the art'survey." International Conference on Entertainment Computing. Springer Berlin Heidelberg, 2008.

[13] S.H. Patel and P.N. Azzam, "Characterization of N200 and P300:Selected Studies of the Event-Related Potential", International Journal of Medical Sciences, pp. 147–154, October 2005.

[14] Annese, V.F., De Venuto, D. "Fall-risk assessment by combined movement related potentials and co-contraction index monitoring". Proceedings - IEEE Biomedical Circuits and Systems Conference: Engineering for Healthy Minds and Able Bodies, BioCAS 2015 - Proceedings, art. 7348366. DOI: 10.1109/BioCAS.2015.7348366 2015.

[15] Annese, V.F., De Venuto, D. "FPGA based architecture for fall-risk assessment during gait monitoring by synchronous EEG/EMG". Proceedings - 2015 6th IEEE International Workshop on Advances in Sensors and Interfaces, IWASI 2015, pp. 116-121. DOI: 10.1109/IWASI.2015.7184953. 2015.

[16] Annese, V.F., De Venuto, D. "Gait analysis for fall prediction using EMG triggered movement related potentials". Proceedings - 2015 10th IEEE International Conference on Design and Technology of Integrated Systems in Nanoscale Era, DTIS 2015, DOI: 10.1109/DTIS.2015.7127386. 2015.

[17] De Venuto, D., Annese, V.F., Ruta, M., Di Sciascio, E., Sangiovanni Vincentelli, A.L. "Designing a Cyber-Physical System for Fall Prevention by Cortico-Muscular Coupling Detection". IEEE Design and Test, 33 (3), art. no. 7273831, pp. 66-76. DOI: 10.1109/MDAT.2015.2480707. 2016.

[18] Annese, V.F., Crepaldi, M., Demarchi, D., De Venuto, D. "A digital processor architecture for combined EEG/EMG falling risk prediction". Proceedings of the Design, Automation and Test in Europe Conference and Exhibition, DATE 2016. 2016.

[19] Annese, V.F., De Venuto, D. "The truth machine of involuntary movement: FPGA based cortico-muscular analysis for fall prevention". 2015 IEEE International Symposium on Signal Processing and Information Technology, ISSPIT 2015, art. no. 7394398, pp. 553-558. DOI: 10.1109/ISSPIT.2015.7394398. 2015.

[20] De Venuto, D., Annese, V.F., Sangiovanni-Vincentelli, A.L. "The ultimate IoT application: A cyber-physical system for ambient assisted living". Proceedings - IEEE International Symposium on Circuits and Systems, pp. 2042-2045. DOI: 10.1109/ISCAS.2016.7538979. 2016.

[21] De Venuto, D., Ohletz, M.J. "On-chip test for mixed-signal ASICs using two-mode comparators with bias-programmable reference voltages". (2001) Journal of Electronic Testing: Theory and Applications (JETTA), 17 (3-4), pp. 243-253. DOI: 10.1023/A:1013377811693. 2001.

[22] De Venuto, D., Carrara, S., Riccò, B. "Design of an integrated low-noise read-out system for DNA capacitive sensors". Microelectronics Journal, 40 (9), pp. 1358-1365. DOI: 10.1016/j.mejo.2008.07.071. 2009.

[23] De Venuto, D., Castro, D.T., Ponomarev, Y., Stikvoort, E. "Low power 12-bit sar adc for autonomous wireless sensors network interface". 3rd International Workshop on Advances in Sensors and Interfaces, IWASI 2009, art. no. 5184780, pp. 115-120. DOI: 10.1109/IWASI.2009.5184780. 2009.

[24] De Venuto, D., Ohletz, M.J., Ricco, B. "Automatic repositioning technique for digital cell based window comparators and implementation within mixed-signal DfT schemes". Proceedings - International Symposium on Quality Electronic Design, ISQED, 2003-January, art. no. 1194771, pp. 431-437. DOI: 10.1109/ISQED.2003.1194771. 2003.

[25] De Venuto, D., Ohletz, M.J., Riccò, B. "Digital window comparator DfT scheme for mixed-signal ICs". Journal of Electronic Testing: Theory and Applications (JETTA), 18 (2), pp. 121-128. DOI: 10.1023/A:1014937424827. 2002.

[26] De Venuto, D., Ohletz, M.J., Riccò, B. "Testing of analogue circuits via (standard) digital gates". Proceedings - International Symposium on Quality Electronic Design, ISQED, 2002-January, art. no. 996709, pp. 112-119. DOI: 10.1109/ISQED.2002.996709. 2002.

[27] D. De Venuto, V. F. Annese, G. Mezzina, M. Ruta, E. Di Sciascio. "Brain-Computer Interface using P300: A Gaming Approach for Neurocognitive Impairment Diagnosis". Proceedings – 2016 IEEE HLDVT, Santa Cruza, USA. ISBN: 978-1-5090-4270-8. 2016.

[28] Nikolay V. Manyakov, et al. , "Comparison of Classification Methods for P300 Brain-Computer Interface on Disabled Subjects," Computational Intelligence and Neuroscience, vol. 2011, Article ID 519868, 12 pages, 2011. doi:10.1155/2011/519868.

[29] De Venuto, D., Vincentelli, A.S. "Dr. Frankenstein's dream made possible: Implanted electronic devices". Proceedings -Design, Automation and Test in Europe, DATE, art. no. 6513757, pp. 1531-1536. 2013.